Chiu and Tandri *Int J Concr Struct Mater* (2020) 14:30
https://doi.org/10.1186/s40069-020-00405-0

International Journal of Concrete Structures and Materials

RESEARCH Open Access

Experimental Investigation on the Force-Crack Quantification Model for HSRC Columns with Flexure–Shear and Shear Failure Modes

Cien-Kuo Chiu* and Alexander Ivan Tandri

Abstract

A total of six full-scale high strength reinforced concrete (HSRC) columns were tested under axial and cyclic lateral loading. The specified concrete compressive strength was 70 MPa and the specified yield strength was 685 MPa and 785 MPa for the longitudinal and transverse reinforcements, respectively. The main variables considered in the study are the transverse reinforcements ratio and axial load ratio. Although such HSRC columns have gradually transformed in use and scope, the damage assessment method is less understood. The main purpose of this study is to propose a damage assessment model for HSRC columns. An analytical backbone curve model for predicting force–deformation behavior of HSRC columns is described. Column stiffness is also measured from the experiment to obtain stiffness reduction factors that are necessary to calculate member deformation. Based on experiment results, a new limiting value of residual crack width is defined to determine damage level. This study uses specified residual crack width of 0.15 mm, 0.30 mm, and 1.00 mm in the damage assessment model. The new limiting value of residual crack width is also used to determine the performance points of structural members. Finally, a new drift ratio limit of each damage level is also proposed. Experiment results are presented and used to investigate the application of the proposed damage assessment model.

Keywords: damage assessment, high strength, reinforced concrete, residual crack

1 Introduction

Reinforced concrete (RC) is the most widely used construction material, owing to its low cost, high durability, easy maintenance, and usefulness in the assembly of building units. However, since it has a higher unit weight and lower strength than steel, few high-rise buildings use RC. Many aging RC structures in Taiwan performed poorly during the 921 Chi–Chi Earthquake of September 21, 1999, leading to a significant decline in the use of this construction material. Relatedly, the use of steel or steel-reinforced concrete (SRC) for high-rise buildings grew rapidly as an alternative. However, the SRC structure is costly and the construction of reinforcing steel bars at the SRC beam-column joint is a complex task. Consequently, a dense arrangement of reinforcements in the limited cross-sectional area may result overcrowding. Briefly, an upgraded RC material that can reduce the size of members and the amount of material needed without loss of safety is required.

The use and definition of high-strength concrete (HSC) has been gradually developing for more than six decades, as mentioned in ACI 363R-10 (2010). Widely available all over the world, HSC has a continuously increasing range of applications, owing to its highly desirable characteristics, such as high early-age strength, low deflections due

*Correspondence: ckchiu@mail.ntust.edu.tw
Department of Civil and Construction Engineering, National Taiwan University of Science and Technology, No. 43, Keelung Road, Daan District, Taipei 10607, Taiwan
Journal information: ISSN 1976-0485 / eISSN 2234-1315

to high modulus elasticity, and high load capacity per unit weight, which allows for the construction of skyscrapers and long bridges. HSC is generally defined as concrete whose compressive strength equals or exceeds 60 MPa and less than 130 MPa, according to FIP/CEB (1990). Along with HSC, high strength reinforcement is increasingly being used in the construction industry. In Taiwan, high-strength reinforced concrete (HSRC) is defined as concrete with a compressive strength that is equal to or higher than 70 MPa and reinforcement steel with a specified yield strength of at least 685 MPa. Additionally, in Taiwan and Japan, HSRC is also referred to as New RC (Chang 2010). However, ACI 318-19 (2019), which is the most common specification that is used in concrete engineering design in Taiwan, limits the specified yielding strength of main bars for column and beam members to 550 MPa. To ensure the reliability of HSRC beam and column members in the performance-based design, a full-size experiment must be conducted to examine continuously their mechanical behavior, especially for damage quantification.

According to the AIJ guidelines (2010), building performance comprises serviceability, safety, and reparability. Restated, along with serviceability and safety, reparability should be considered in the performance-based design of buildings. Moreover, the assessment of damage is critical in estimating the reparability of a building. Despite the considerable attention that is paid to methods for assessing damage to an RC member or structure, most of such investigations have focused on normal-strength RC (NSRC), while only a few have considered HSRC structural members.

Besides reparability, a damage assessment can also be used to estimate the residual seismic capacity of structures after an earthquake. In Japan, the Japan Building Disaster Prevention Association (JBDPA 2001) provides technical guidelines for the evaluation of the residual seismic capacity of earthquake-damaged reinforced concrete buildings for engineers and inspectors. JBDPA (2001) specifies five levels of structural damage of an RC member, which are presented in Table 1. Based on the definition in Table 1, the damage level should be determined from the maximum residual crack width, concrete stress, steel stress, and member strength, as shown in Table 2.

Table 3 presents the seismic capacity reduction factors for various RC vertical components. JBDPA (2015) included a seismic capacity reduction factor for a column member under flexure–shear failure, which was not provided in JBDPA (2001).

Chiu et al. (2014) concluded that since an increase in the strength of concrete and steel significantly affects the crack formation of structural members under lateral loads, the damage development of HSRC members differs

Table 1 Definition of damage levels of structural members.

Damage level	Description of damage
I	Visible narrow cracks on concrete surfaces. Crack widths are less than 0.2 mm
II	Visible cracks on concrete surfaces. Cracks widths range from about 0.2 mm to 1.0 mm
III	Noticeable wide cracks. Cracks widths range from about 1.0 mm to 2.0 mm. Localized crushing of concrete cover
IV	Crack widths are greater than 2 mm. Crushing of concrete with exposed reinforcing bars. Spalling of concrete cover
V	Buckling of reinforcing bars. Crushing of core concrete. Visible vertical deformation in column and/or shear walls. Side-sway, subsidence of upper floors, and/or fracture of reinforcing bars are observed in some cases

Table 2 Determination of damage level (AIJ 2010; JBDPA 2001).

Damage level	Maximum residual crack width	Concrete stress	Steel stress	Member strength
I (slight)	0–0.2 mm			
II (light)	0.2–1 mm	Concrete cover $> 2/3\ f_c'$	Yielding	
III (moderate)	1–2 mm	Concrete cover $> f_c'$		
IV (severe)	> 2 mm	Concrete core Maximum strength		Maximum Strength of the member
V (collapse)				The member is unable to resist axial load or its capacity is less than 80%

Table 3 Seismic reduction factors suggested by JBDPA (2001).

Damage level	RC column			RC wall		RC beam	
	Shear	Flexure–shear	Flexure	Shear	Flexure	Shear	Flexure
I	0.95	0.95	0.95	0.95	0.95	0.95	0.95
II	0.6	0.7	0.75	0.6	0.7	0.7	0.75
III	0.3	0.4	0.5	0.3	0.4	0.4	0.5
IV	0	0.1	0.2	0	0.1	0.1	0.2
V	0	0	0	0	0	0	0

from that of NSRC. Therefore, the conventional damage assessment model for NSRC members may be useless for evaluating the performance of HSRC members or structures. Few full-size experimental studies have focused on quantification of the damage of HSRC column members. Since the mechanical behavior of the shear-critical HSRC column members is more complex than that of HSRC column members in flexural failure mode, six full-size HSRC column specimens with flexure–shear and shear failure modes are used to develop a damage quantification model based on the experimental investigation herein. Furthermore, in order to simulate the actual conditions of structural columns in a building, the loading system that is used in this work will deform specimens with double curvature under displacement control.

Santoro and Kunnath (2013) stated that damage assessment for an RC frame is rather complex even using the most advanced and computationally demanding modeling strategies, as it involves material and geometrical nonlinearities in both concrete and reinforcing steel. However, a simplified damage assessment method that is based on experimental results is necessary for practical damage-controlling design. Therefore, this work develops a novel damage quantification model that can be used to elucidate the development of damage in HSRC column members with flexure–shear and shear failure modes under cyclic loading. Additionally, the proposed model can be used to plot the relationships between force, deformation, and damage level, which are required to capture the detailed damage process. Since damage to HSRC columns should be quantified using the maximum residual crack width, a force-crack model that can estimate the maximum residual crack width from an applied lateral force is also developed. Finally, the proposed model is used to plot a figure of the detailed damage process for each specimen in Fig. 1, which includes the relationship curves of the force vs. deformation, force vs. residual crack width, damage level as a function of residual crack width, and damage level as a function of deformation. Using the relationship curves in quadrants of I and IV, engineers can set an allowable damage level from which they can determine the corresponding allowable force and deformation under cyclic loading. The relationship curves in quadrants of II and III can help engineers to identify the damage level in a post-earthquake performance assessment.

2 Experimental Setting and Results

2.1 Full-Scale Experiment on HSRC Column Members

Six full-size HSRC column specimens with a specified concrete compressive strength of at least 70 MPa and high-strength reinforcement are tested under cyclic loading and similar with research by Chiu et al. (2019). The cross-sectional area of each specimen is 600×600 mm and its clear height is 1800 mm. The diameter of the longitudinal reinforcements in these specimens is 29 mm with a specified yielding strength of 685 MPa and the diameter of transverse reinforcements is 13 mm with a specified yielding strength of 785 MPa. The major differences between these specimens are in the spacing of transverse reinforcements and the applied axial loading. Table 4 and Fig. 2 present the detailed arrangement of the reinforcements (Chiu et al. 2019).

2.2 Test Procedure

In the experiment by Chiu et al. (2019), the Multi-Axial Testing System (MATS) is used to damage a specimen gradually with displacement control. Lateral and axial loadings are applied to each specimen, as shown in Fig. 3. A MATS machine can deform a specimen with double curvature, as found in a real RC building structure. Figure 4 presents the loading cycle in detail.

To measure the crack width, the specimens are brushed using white paint and covered with a 100×100 mm grid. Strain gauges are installed on the actual longitudinal bars on the flexure side and the actual transverse bars on the shear side. The position of the strain gauges is also marked on the column face. Since the specimens are deformed with double curvature under cyclic loading, the flexural cracks on the bottom part of the specimen are assumed to be the same as those on the top part. Therefore, during the

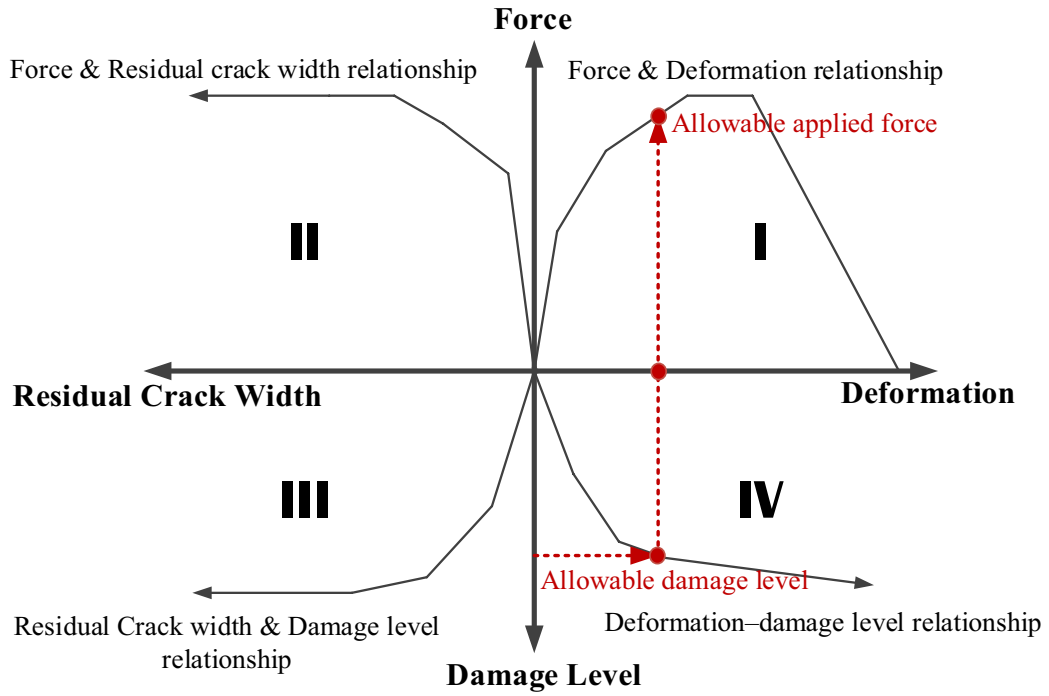

Fig. 1 Detailed damage process of a column member.

Table 4 Detailed design information of each specimen (Chiu et al. 2019).

Design parameters	10S0.15	10S0.30	15S0.15	15S0.30	20S0.15	20S0.30
Width (mm)	600	600	600	600	600	600
Depth (mm)	600	600	600	600	600	600
f_c' (MPa)	88	74	87	76	77	71
f_{yl}' (MPa)	716	716	716	716	716	716
f_{yt}' (MPa)	858	858	858	858	858	858
ρ_l (%)	3.37	3.37	3.37	3.37	3.37	3.37
ρ_t (%)	1.08	1.08	0.72	0.72	0.54	0.54
P_r	0.15	0.30	0.15	0.30	0.15	0.30
s (mm)	100	100	150	150	200	200

f_c' is the concrete compressive strength; f_{yl}' is the longitudinal bar yield strength; f_{yt}' is the transverse bar yield strength; ρ_l is the longitudinal bar ratio; ρ_t is the transverse bar ratio; P_r is the axial load ratio; s is the spacing of transverse bar.

experiment, only the flexural cracks on the bottom half of the column are measured. These flexural cracks are measured at two positions—where the flexural crack is widest and at the intersection between the longitudinal reinforcement and the flexural crack. The shear cracks are also measured at two positions—where the shear crack is widest and at the intersection between the shear crack and transverse reinforcement. Figure 5 displays the measurement of flexural and shear cracks.

2.3 Experiment Results and Damage Identifications

2.3.1 Force–Deformation Relationship and Crack Development of Specimens

Figure 6 plots the relationship between the lateral force and deformation of each specimen, obtained using the applied loading system, which was introduced in Sect. 2.2. To determine the damage state of each specimen, it is returned to zero deformation from a specific peak drift ratio and the residual crack width is measured. Figure 7 plots the maximum residual flexural

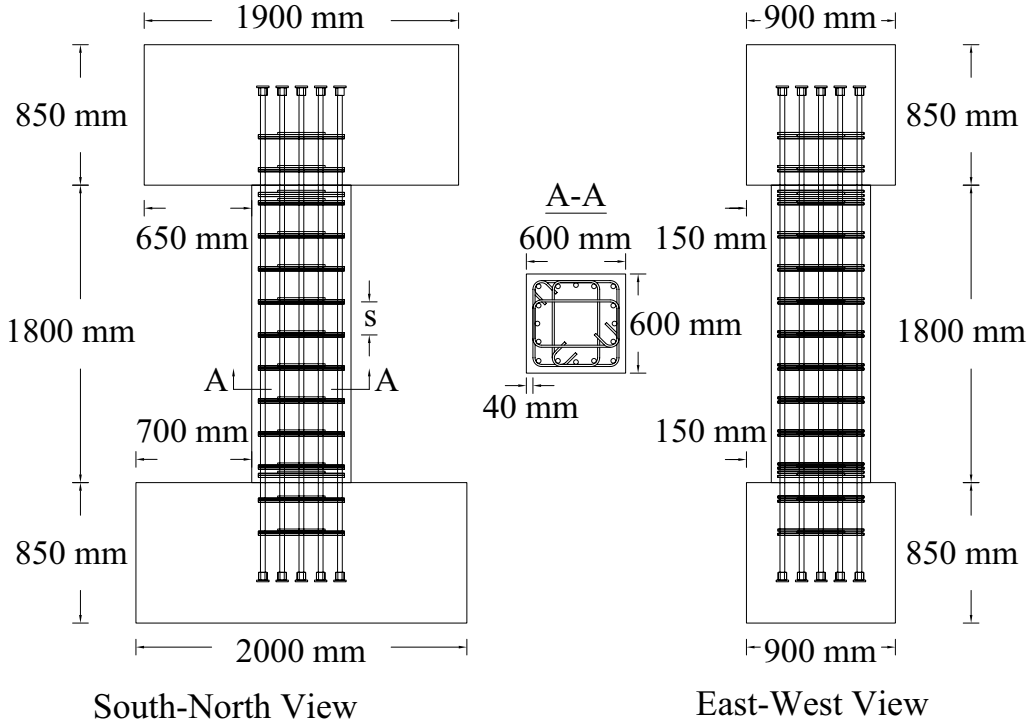

Fig. 2 Typical reinforcement arrangements of the specimen (Chiu et al. 2019).

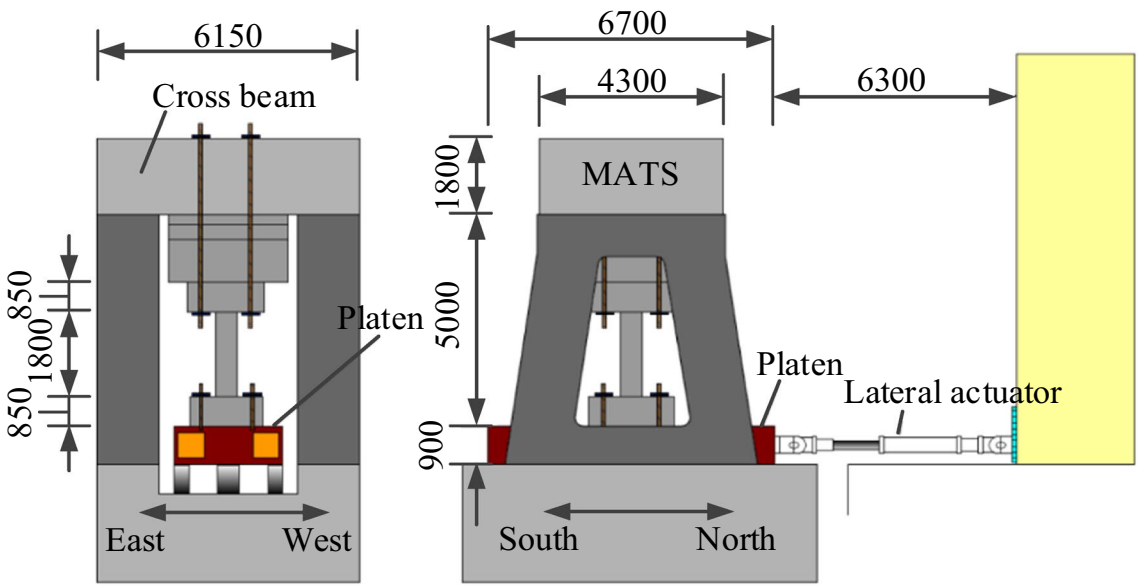

Fig. 3 Layout of Multi-Axial Testing System (MATS).

crack width and maximum residual shear crack width for each specimen under applied loading. The residual shear crack dominates the crack development in each specimen. Therefore, the maximum residual shear crack width can be used to construct the force-crack model in the sequent section. Based on the experimental results,

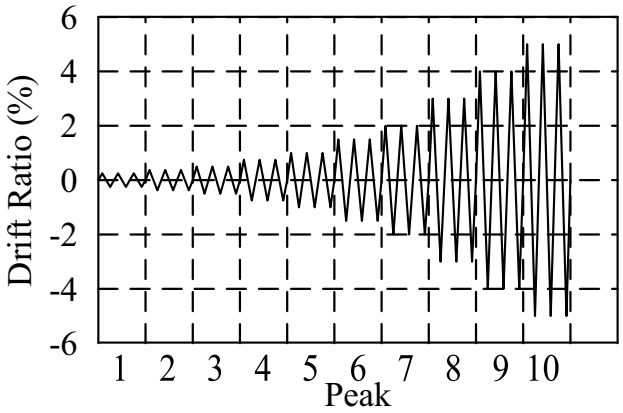

Peak	Drift Ratio (%)	Peak	Drift Ratio (%)
1	0.25	6	1.5
2	0.375	7	2
3	0.5	8	3
4	0.75	9	4
5	1	10	5

Fig. 4 Cyclic loading protocol in the experiment.

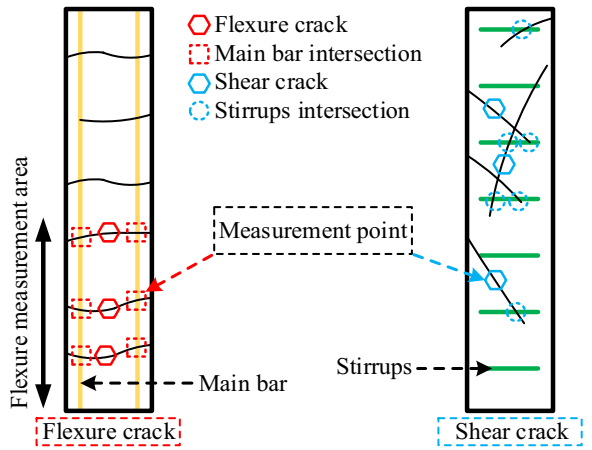

Fig. 5 Measuring cracks of various types at various positions in a specimen.

Table 5 presents detailed information concerning the specified performance points of each specimen, such as the cracking point, the yielding point, and the maximum strength point.

2.3.2 Identification of Damage of Specimens

2.3.2.1 (a) 10s0.15 At a deformation of +0.375% (1st cycle), slight cracks appear on the concrete surface so the specimen exhibits damage level I under this deformation. As the drift ratio increases, the flexural crack width and shear crack width also increase, but not significantly. At a deformation of +1% (1st cycle), the maximum residual flexural crack width and shear crack width reach 0.25 mm and 0.1 mm, respectively, and the main bars and stirrups have not yielded. Therefore, the damage level is controlled by the maximum residual crack width and the specimen exhibits damage level II under this deformation. At a deformation of +1.5%, the widths of flexural and shear cracks increase and some concrete near the top of the foundation is crushed. Since the stress of the concrete cover exceeds the compressive strength of concrete, f_c', this deformation corresponds to damage level III. At a deformation of 2% (1st cycle), the specimen reaches its maximum strength and the widths of the shear cracks increase significantly; the maximum residual shear crack width is over 2.0 mm. Moreover, the concrete cover close to the bottom and top ends of the specimen spall. This deformation corresponds to damage level IV. At the same deformation in the third cycle, the maximum residual shear crack width increases significantly, reaching 4.5 mm. At a deformation of 5% (1st cycle), the concrete cover spalls severely along the column, as presented in Fig. 8. Since the strength is less than 60%, the experiment is terminated. Based on the damage pattern, the failure mechanism of this specimen is flexure–shear.

2.3.2.2 (b) 10s0.30 A shear crack develops at a deformation of +0.5% (1st cycle), at which the maximum residual crack width is only 0.02 mm. Since the maximum residual crack width is less than 0.2 mm, this deformation corresponds to damage level I. At a deformation of +0.75% (1st cycle), the crack width increases, but not critically as the maximum residual crack width is 0.26 mm. At this deformation, the stirrups have yielded. Therefore, based on the definition of damage level by AIJ (2010) and JBDPA (2001), this drift ratio corresponds to damage level II. At a deformation of +1% (1st cycle), the maximum residual crack width reaches 0.3 mm with some localized crushing of the concrete cover near the top of the column. This deformation corresponds to damage level III. At a deformation of 1.5% (1st cycle), the maximum residual crack width is 1.5 mm. The column is also heavily damaged by the applied axial load and the concrete cover has spalled severely. Based on the provided definition, this drift ratio

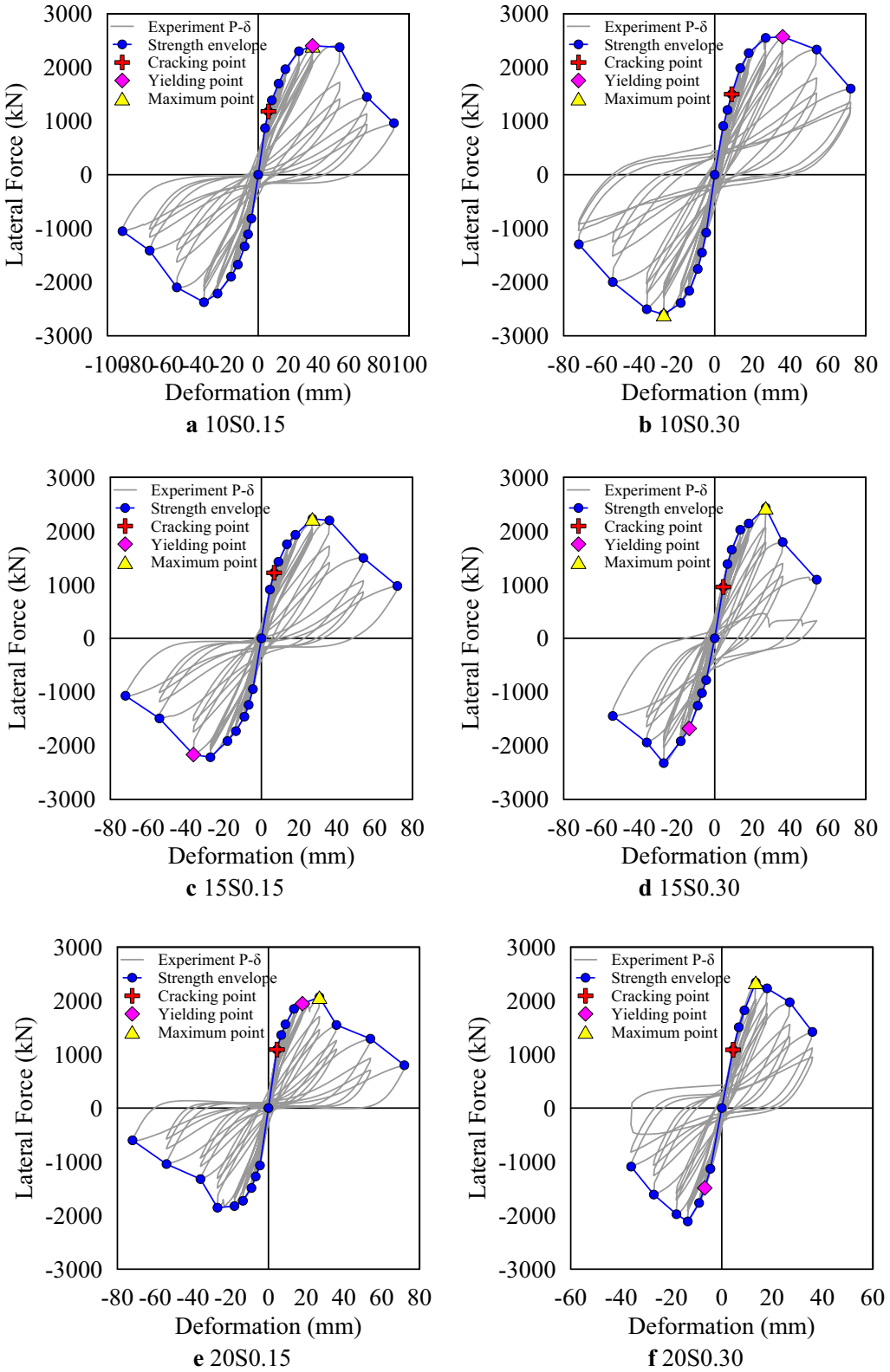

Fig. 6 Relationship of lateral force and deformation for each specimen.

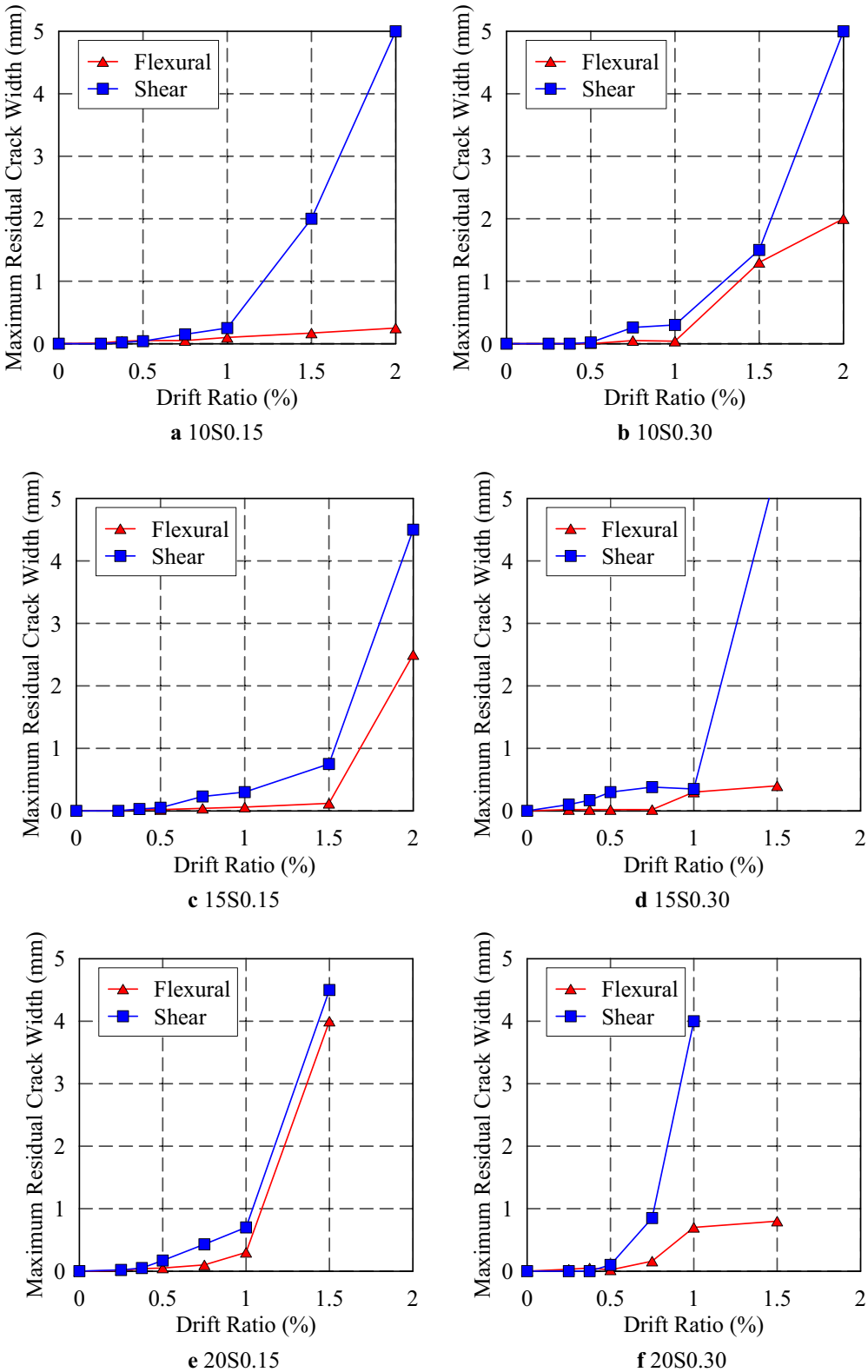

Fig. 7 Residual crack development for each specimen.

Table 5 Drift ratios related to the initial crack, yielding occurrence of the reinforcement, and final step (Chiu et al. 2019).

Specimen	Initial flexural crack	Initial shear crack	Initial yielding of main bars	Initial yielding of stirrups	Maximum strength point	0.8 maximum strength point (%)	Final step (%)
10S0.15	+0.375% (1st cycle)	+0.375% (1st cycle)	+2.0% (1st cycle)	+2.0% (1st cycle)	+2.0% (1st cycle)	3.16	−5
10S0.30	+0.75% (3rd cycle)	+0.50% (1st cycle)	+2.0% (1st cycle)	+0.75% (1st cycle)	−1.5% (1st cycle)	2.61	−4
15S0.15	+0.375% (1st cycle)	+0.375% (1st cycle)	−2.0% (2nd cycle)	−0.75% (2nd cycle)	+1.5% (1st cycle)	2.48	−4
15S0.30	+0.25% (1st cycle)	+0.25% (1st cycle)	−0.75% (1st cycle)	+0.375% (1st cycle)	+1.5% (1st cycle)	1.71	−3
20S0.15	+0.25% (1st cycle)	+0.25% (1st cycle)	+1.0% (2nd cycle)	−1.0% (3rd cycle)	+1.5% (1st cycle)	1.83	−4
20S0.30	+0.25% (1st cycle)	+0.50% (1st cycle)	−0.375% (3rd cycle)	+1.0% (1st cycle)	+0.75% (1st cycle)	1.36	−2

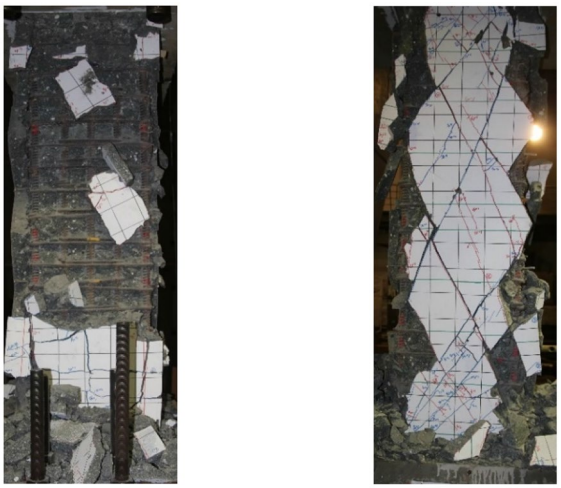

Fig. 8 Damage state of the specimen of 10S0.15 at the final step.

Fig. 9 Damage state of the specimen of 10S0.30 at the final step.

corresponds to damage level IV. This column reaches its maximum strength at a deformation of −1.5% (1st cycle). This specimen reaches the final step of loading at a deformation of −4% (3rd cycle), at which the concrete cover on the flexure side and the shear side of the specimen are seriously damaged (Fig. 9). The damage on the flexure side is mostly caused by flexural cracking and cracking that induced by a high axial load. Therefore, the experiment is terminated at this point. Based on the damage pattern, the failure mechanism of this column is flexure–shear.

2.3.2.3 (c) 15s0.15 The flexural crack and shear crack develop at a deformation of +0.375% (1st cycle). At a deformation of +0.75% (1st cycle), the maximum residual shear crack width increases significantly, reaching 0.23 mm, and the maximum flexural crack width remains only 0.04 mm. In the 2nd cycle of this deformation, the stirrups yield. This point corresponds to damage level II. At a deformation of 1%, the maximum residual crack width is 0.3 mm, and this deformation corresponds to damage level II. At a deformation of 1.5% (1st cycle), which is also the maximum strength point of the specimen, the maximum residual crack width is 0.35 mm. Since the specimen reaches its maximum strength point, this deformation corresponds to a damage level of IV. In the 3rd cycle at the same drift ratio, the maximum crack width significantly increases, reaching 0.75 mm. This specimen reaches the final step of loading at a deformation of −4% (1st cycle). At this deformation, the flexure side is damaged severely by flexural cracking and cracking that is induced by the

a Flexure Side b Shear Side

Fig. 10 Damage state of the specimen of 15S0.15 at the final step.

axial load, and the shear side is also seriously damaged by the shear crack (Fig. 10). Since the member strength is less than 60% of the maximum strength, the experiment is terminated. Based on the damage pattern, the failure mechanism of this specimen is shear failure.

2.3.2.4 (d) 15s0.30 At a deformation of +0.25% (1st cycle), slight cracks develop on the flexure side and the shear side. This deformation corresponds to damage level I. At a deformation of +0.375% (1st cycle), the stirrups yield but the maximum residual crack width is still less than 0.2 mm. This deformation corresponds to damage level II. At a deformation of +0.5% (1st cycle), the concrete cover on the corner of the column spalls because the surface of the foundation is not sufficiently flat. Therefore, when loading is applied using the MATS, the column experiences a twist moment and the stress on one of the corner areas is relatively high and causes the concrete cover in the corner to spall. However, despite the spalling of the concrete cover on the corner of the column, the maximum crack width is only 0.18 mm. At a deformation of +0.75% (1st cycle), the maximum residual crack width is 0.3 mm and some localized crushing occurs on the column surface. Therefore, this deformation corresponds to damage level III. At a deformation of +1% (1st cycle), the maximum crack width is still less than 1 mm, while the number of shear cracks is significantly increased. This deformation still corresponds to damage level III. At a deformation of +1.5% (1st cycle), which is the maximum strength point, the maximum residual crack width is increased significantly to 1 mm. Since the column reaches its maximum strength point, this deformation corresponds to damage level IV. In the 3rd cycle of the same deformation, the maximum residual crack width increases significantly, reaching 5.5 mm. Beyond this drift ratio, the maximum residual crack width is controlled by shear cracking. At a deformation of +3% (2nd cycle), the column reaches its final step of loading. The shear side and the concrete cover on the flexure side are severely damaged by the high axial load (Fig. 11). Since member strength is less than 60% of maximum strength, the experiment is terminated. Based on the damage pattern, the failure mechanism of the column is identified as shear failure.

2.3.2.5 (e) 20s0.15 Some slight shear and flexural cracking develop at a deformation of +0.25% (1st cycle). As the drift ratio increases, the maximum residual crack width also increases, but not critically up to a deformation of +1% (1st cycle). At a deformation of +1% (1st cycle), the maximum residual shear crack width reaches 0.45 mm, and the maximum residual flexural crack width is still 0.22 mm. Therefore, the maximum residual shear crack width determines the maximum residual crack width. At this deformation, small spalling occurs on the compression side. Therefore, at this point, the column is at damage level III. The maximum strength point of this column is reached at a deformation of 1.5% (1st cycle). The maximum residual shear crack width increases significantly, reaching 2.5 mm. This deformation corresponds to a damage level of more than IV. In the 3rd cycle of the same deformation, the maximum residual crack width increases significantly, reaching 4 mm. The measurement of the crack widths is no longer necessary at this deformation. The experiment continues until the final step of loading is reached at a deformation of −4% (1st cycle). The concrete cover on the flexure side at the middle span spalls severely

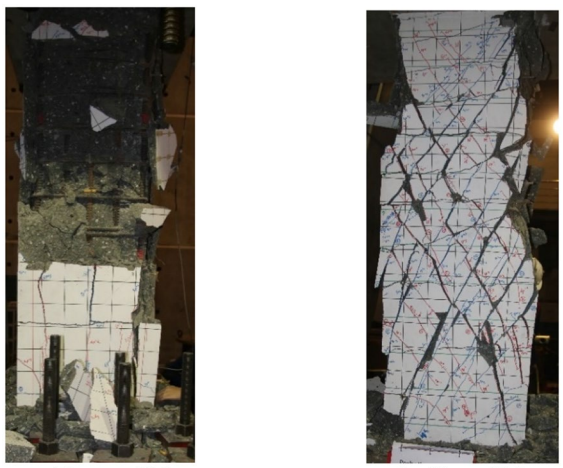

a Flexure Side b Shear Side

Fig. 11 Damage state of the specimen of 15S0.30 at the final step.

a Flexure Side b Shear Side

Fig. 12 Damage state of the specimen of 20S0.15 at the final step.

a Flexure Side b Shear Side

Fig. 13 Damage state of the specimen of 20S0.30 at the final step.

and the shear side is also seriously damaged by the shear cracking (Fig. 12). Since the member strength is less than 60% of maximum strength, the experiment is terminated. Based on the damage pattern, the failure mechanism is identified as shear failure.

2.3.2.6 (f) 20s0.30 The flexural cracking develops at a deformation of +0.25% (1st cycle). The main bar has yielded at a deformation of −0.375% (3rd cycle), while the maximum crack width is still less than 0.2 mm. This deformation corresponds to damage level II. At a deformation of +0.5% (1st cycle), the shear crack begins to develop and the maximum residual crack width does not exceed 0.2 mm. At a deformation of +0.75% (1st cycle), which is the maximum strength point, the shear crack widths increase significantly. The concrete cover close to the bottom of the column has spalled but the maximum residual crack width that corresponds to this point is only 0.43 mm. This deformation corresponds to damage level IV. Beyond this drift ratio, the maximum residual crack width increases significantly and the damage level exceeds level IV. However, the experiment is continued without measuring the crack widths. At a deformation of −2% (3rd cycle), this column reaches its final step of loading. The concrete spalls severely along the column and some of the main bars buckle (Fig. 13). Therefore, the experiment is terminated. Based on the damage pattern, the failure mechanism of this column is identified as shear failure.

To simplify the determination of the damage level of HSRC column member with the flexure–shear or shear failure mode, this work uses a criteria that are based on the maximum residual crack width. The authors have developed a limiting values of maximum residual crack width for each damage level (Chiu et al. 2019). Since specimen 15S0.30 underwent twist moment loading in the experiment, only data on five of the six specimens are used to investigate the determination of the damage level. The average values of the maximum residual crack width of the selected specimens are used to determine the limiting and suggested values of maximum residual crack width for each damage level. Table 6 presents the limiting value of the maximum residual crack width for each damage level for each column and the average and suggested values of maximum residual crack width. In the following analysis, the damage level of an HSRC column member with the flexure–shear or shear failure mode is determined based on the maximum residual crack width, as suggested herein.

3 Simulation Model of Mechanical Behavior

3.1 Analytical Model for Force–Deformation Relationship

A monotonic force–deformation relationship of a structural member is essential to understand its performance under seismic loading and serves as a primary backbone curve to characterize the failure mode of a member. This work concerns HSRC column members with flexure–shear failure and shear failure. Generally, flexure–shear failure members reach their maximum strength after the yield of their longitudinal reinforcements. Once the specimens have reached their maximum strength, the significant transverse reinforcements enable their flexural strength to be maintained before shear failure. However, shear failure members typically reach their maximum strength before the longitudinal reinforcements yield. After the maximum point has been reached, the strength

Table 6 Maximum residual crack widths for each damage level (Chiu et al. 2019).

Damage level	Specimen					Average value (mm)	Suggested value (mm)
	10S0.30 (mm)	10S0.15 (mm)	15S0.15 (mm)	20S0.30 (mm)	20S0.15 (mm)		
I	< 0.11	< 0.16	< 0.23	< 0.06	< 0.25	0–0.16	0–0.15
II	0.11–0.30	0.16–0.29	0.23–0.35	0.06–0.45	0.25–0.45	0.16–0.35	0.15–0.30
III	0.30–1.05	0.29–2.1	N/A	N/A	0.45–2.5	0.35–1.29	0.30–1.0
IV	> 1.05	> 2.1	> 0.35	> 0.45	> 2.5	> 1.29	> 1.0

decreases rapidly to a point that is defined as the axial failure point.

The behavior of HSRC structural members differs from that of NSRC members. Therefore, a model that describes the force–deformation relationship of HSRC members is needed. Sezen (2002) proposed a piecewise linear model of force–deformation response, which combines flexural, slip, and shear deformation. Using modified compression field theory, Setzler (2005) defined the force–deformation relationship up to the maximum strength. Using the same piecewise linear model as Sezen (2002), Patwardhan (2005) suggested a different model for use beyond the maximum point. Maekawa and An (2000) suggested shear strength degradation after the maximum point. Yoshimura and Takaine (2005) introduced force–deformation models for RC column members with shear failure and flexural failure modes. Based on research on RC column members with shear failure and flexural failure modes, in this work, the flexure–shear failure model includes four points (cracking point, maximum strength point, flexure–shear point, and axial failure point) and the shear failure model includes three points (cracking point, maximum point, and axial failure point), as shown in Fig. 14.

3.1.1 Cracking Point

At the cracking point, a member starts to form either flexural cracks or shear cracks. Cracking strength is the smaller of flexural cracking strength, V_{fc}, and shear cracking strength, V_{sc}. Cracking strength is calculated using Eqs. (1) to (3).

$$V_{cr} = \min\left(V_{fc}, V_{sc}\right) \tag{1}$$

$$V_{fc} = \frac{2M_{cr}}{L} = \frac{2f_r I_g}{Ly_t} \tag{2}$$

$$V_{sc} = \frac{bh}{1.5}\sqrt{f_t^2 + f_t \times f_o} \tag{3}$$

where M_{cr} is the cracking moment; f_r is the concrete rupture stress ($0.97\sqrt{f_c'}$); I_g is the moment inertia of gross section; L is the clear span of the member; y_t is the distance from neutral axis to outermost tension side; f_t is the

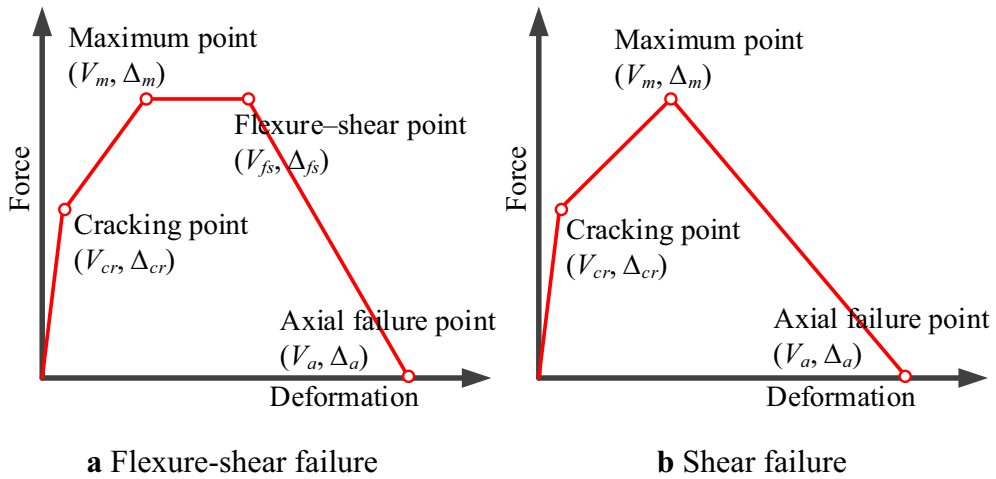

a Flexure-shear failure **b** Shear failure

Fig. 14 Force–deformation model for flexure–shear failure and shear failure.

concrete tensile strength ($0.33\sqrt{f_c'}$); f_o is the applied axial stress that should not exceed 10 MPa (AIJ 2010).

Furthermore, the axial load substantially influences crack development in the early loading stage. Members under a relatively low axial load form cracks more easily than those under high axial load. Table 7 shows the cracking strength of each specimen.

The deformation of a member at the cracking point is calculated using Eq. (4).

$$\Delta_{cr} = \frac{V_{cr}}{\varphi_{cr} K} \tag{4}$$

where K is the theoretical stiffness and is calculated using Eq. (5); ϕ_{cr} is the stiffness reduction factor for the cracking point.

$$K = \frac{k_f \times k_s}{k_f + k_s} \tag{5}$$

where k_f is the flexural stiffness of a member with the double curvature, $12EI/L^3$ and ks is the shear stiffness of a member with the double curvature, $GA/(L\kappa)$; G is the shear modulus of concrete; κ is the shape factor, can be taken as 1.2. However, the stiffness that is calculated using Eq. (5) exceeds the experimentally determined actual stiffness. Therefore, a stiffness reduction factor is introduced and obtained from experimental results.

3.1.2 Maximum Strength Point

The maximum strength point in the backbone curve of a column member is determined by the failure mode—flexure–shear failure or shear failure. Restated, the maximum strength point should be determined by considering the shear force that corresponds to the flexural capacity and the shear capacity of a column member. The flexural capacity of a column member, M_b, is calculated using the equivalent block of effective stress in which the concrete strain at the outermost compressive fiber is assumed to be 0.003. Figure 15 presents the assumed stress and strain distributions in a section for the purposes of calculating flexural capacity. According to NCREE guidelines (2017), for an HSRC column member, α_1 and β_1 are calculated using Eqs. (6) and (7) respectively. The shear force that corresponds to the

Table 7 Cracking strength for each specimen.

Cracking point	Specimen					
	10S0.15	10S0.30	15S0.15	15S0.30	20S0.15	20S0.30
V_{fc}	1001	1355	992	1382	1175	1306
V_{sc}	1528	1449	1523	1461	1467	1431
V_{cr}	1001	1355	992	1382	1175	1306

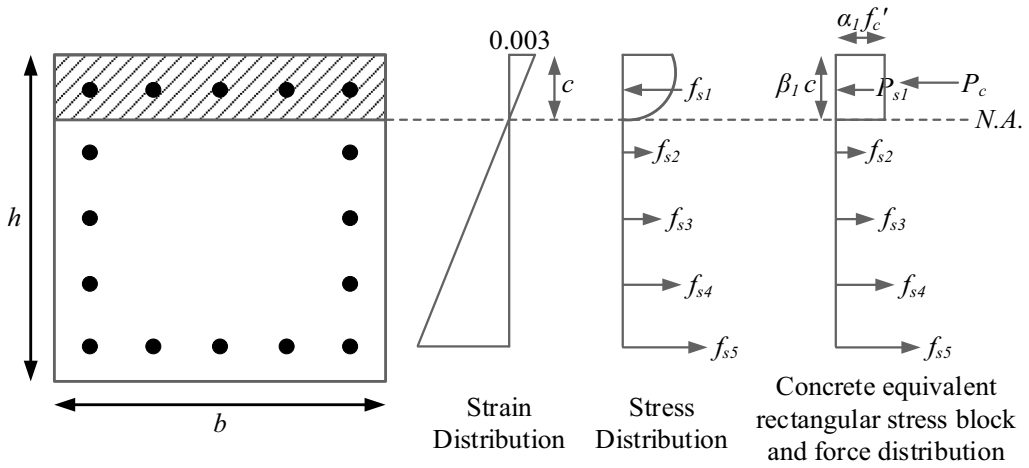

Fig. 15 Stress and strain distributions of a section for the flexural capacity calculation.

flexural capacity of a column member with double curvature, V_b, is calculated using Eq. (8).

$$0.7 \le \alpha_1 = 0.85 - 0.0022\left(f_c' - 55\right) \le 0.85 \tag{6}$$

$$\beta_1 = \begin{cases} 0.85 & f_c' \le 27.5\,\text{MPa} \\ 0.85 - 0.0073\left(f_c' - 27.5\right) & 27.5\,\text{MPa} < f_c' \le 55\,\text{MPa} \\ 0.65 & f_c' > 55\,\text{MPa} \end{cases} \tag{7}$$

$$V_b = \frac{2M_b}{L} \tag{8}$$

For a column member, its shear strength, V_n, is contributed from the shear strength of concrete, V_c, and transverse reinforcements, V_s, respectively. This work adopts Eqs. (9) to (11) to calculate V_n based on the recommendation of NCREE (2017).

$$V_n = V_c + V_s \tag{9}$$

$$V_c = 0.17\left(1 + \frac{P}{14A_g}\right)\sqrt{f_c'}bh \tag{10}$$

$$V_s = \frac{A_{st}f_{yt}d_c}{s} \tag{11}$$

where P is the axial load applied on a column member; A_g is the sectional area of column; A_{st} is the area of transverse reinforcement; f_{yt} is the yield stress of transverse reinforcement, that is limited to 600 MPa; d_c is the effective depth of a section; s is the spacing of transverse reinforcement. According to Fig. 16, the maximum strength point of a column member is calculated using Eq. (12). Its corresponding deformation at the maximum strength point is calculated using Eq. (13).

$$V_m = \min(V_b, V_n) \tag{12}$$

$$\Delta_m = \frac{V_m}{\varphi_m K} \tag{13}$$

where ϕ_m is the stiffness reduction factor for the maximum strength point, which can be identified based on the experiment results. Moreover, Table 8 shows the maximum strength of each specimen.

3.1.3 Flexure–Shear Failure Point

When a column member has significant transverse reinforcements, its flexural strength can be sustained before

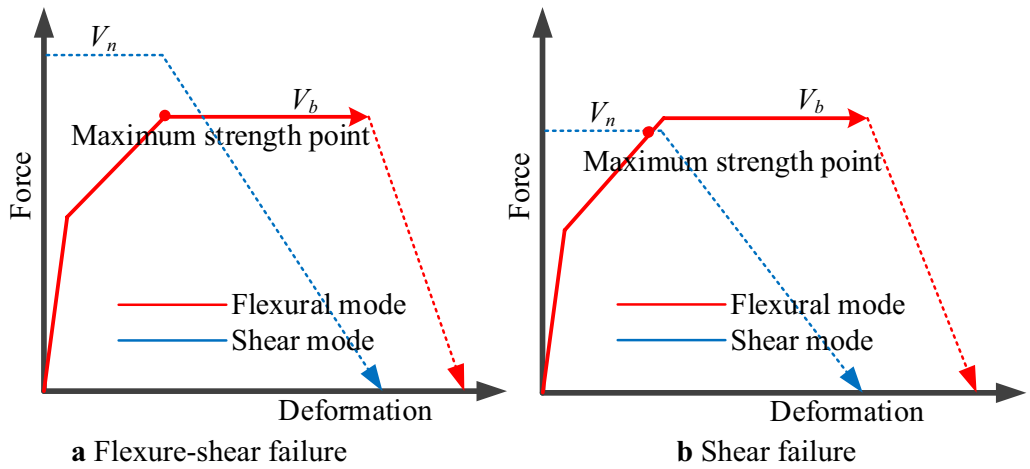

Fig. 16 Definition of maximum point for flexure–shear failure and shear failure.

Table 8 Maximum strength for each specimen.

Maximum point	Specimen					
	10S0.15	10S0.30	15S0.15	15S0.30	20S0.15	20S0.30
V_b	2641	2454	2628	2481	2495	2411
V_n	2735	2976	2177	2471	1783	2097
V_m	2641	2454	2177	2471	1783	2097

shear failure. According to research by Elwood and Moehle (2005), the deformation of a column member that corresponds to this point is given by Eq. (14).

$$\frac{\Delta_{fs}}{L} = \frac{3}{100} + 4\rho'' - \frac{1}{133}\frac{v_m}{\sqrt{f'_c}} - \frac{1}{40}\frac{P}{A_g f'_c} \geq \frac{1}{100} \quad (14)$$

where ρ'' is the volume ratio of transverse reinforcement ($A_{st}/(b \times s)$); v_m is the shear stress of a section ($v_m = V_m/(bh)$).

3.1.4 Axial Failure Point

For a column member, as deformation increases, its lateral strength decreases to zero, when its axial capacity is lost. This point is specified as the axial failure point. According to Elwood and Moehle (2005), the deformation at this point is given by Eq. (15). For a column member with shear failure, the deformation at this point is limited to $0.04L$.

$$\Delta_a = \frac{4}{100} L \frac{1 + (\tan\alpha)^2}{\tan\alpha + P\left(\frac{s}{A_{st} f_{yt} d_c \tan\alpha}\right)} \quad (15)$$

where α is the crack angle of a failure plane and can be estimated using $45° - 35° \times P/P_o$ (P_o is the axial capacity of a column member); s is the spacing of transverse reinforcement; A_{st} is the area of transverse reinforcement; f_{yt} is the yield stress of transverse reinforcement.

3.1.5 Stiffness Reduction Factor

As mentioned before, a reduction factor must be applied to reduce the stiffness so that it matches the experimental results. Based on research by Maeda and Kang (2009), such a reduction factor is highly correlated with the axial load ratio and the transverse reinforcement ratio. Regression analysis can be used to obtain the reduction factors for the cracking point and the maximum strength point, which are given by Eqs. (16) and (17). Figure 17 compares the measured and predicted stiffness reduction factors.

$$\varphi_{cr} = 0.562P_r - 0.210\rho_t + 0.458 \quad (16)$$

$$\varphi_m = 0.705P_r - 0.238\rho_t + 0.245. \quad (17)$$

3.2 Proposed Monotonic Model of a Force–Deformation Relationship

This section summarizes the results that are obtained using the proposed monotonic model of a force–deformation relationship for each specimen, as shown in Fig. 18. The model assumes symmetrical behaviors under positive and negative loading. Table 9 presents the measured and predicted forces when the first crack occurs. As stated in Sect. 2.3.2, specimen 15S0.30 undergoes twist moment loading and the predicted force at the cracking point has a relatively large error. Table 10 presents the measured and predicted forces at the maximum strength point. The maximum strength can be predicted accurately and conservatively, except for specimens 10S0.15 and 15S0.30. As stated in Sect. 3.1, specimens 10S0.15 and 10S0.30 exhibit flexure–shear failure whereas specimens 15S0.15, 15S0.30, 20S0.15, and 20S0.30 exhibit shear failure.

In order to identify the relationship between the residual deformation and the applied force, the unloading stiffness is investigated with reference to the

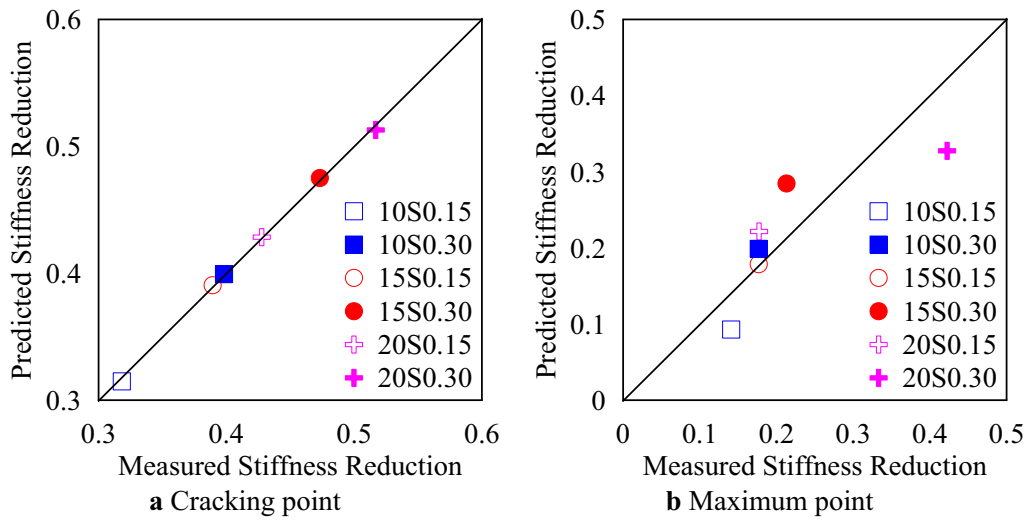

Fig. 17 Comparison of measured and predicted stiffness reduction factors.

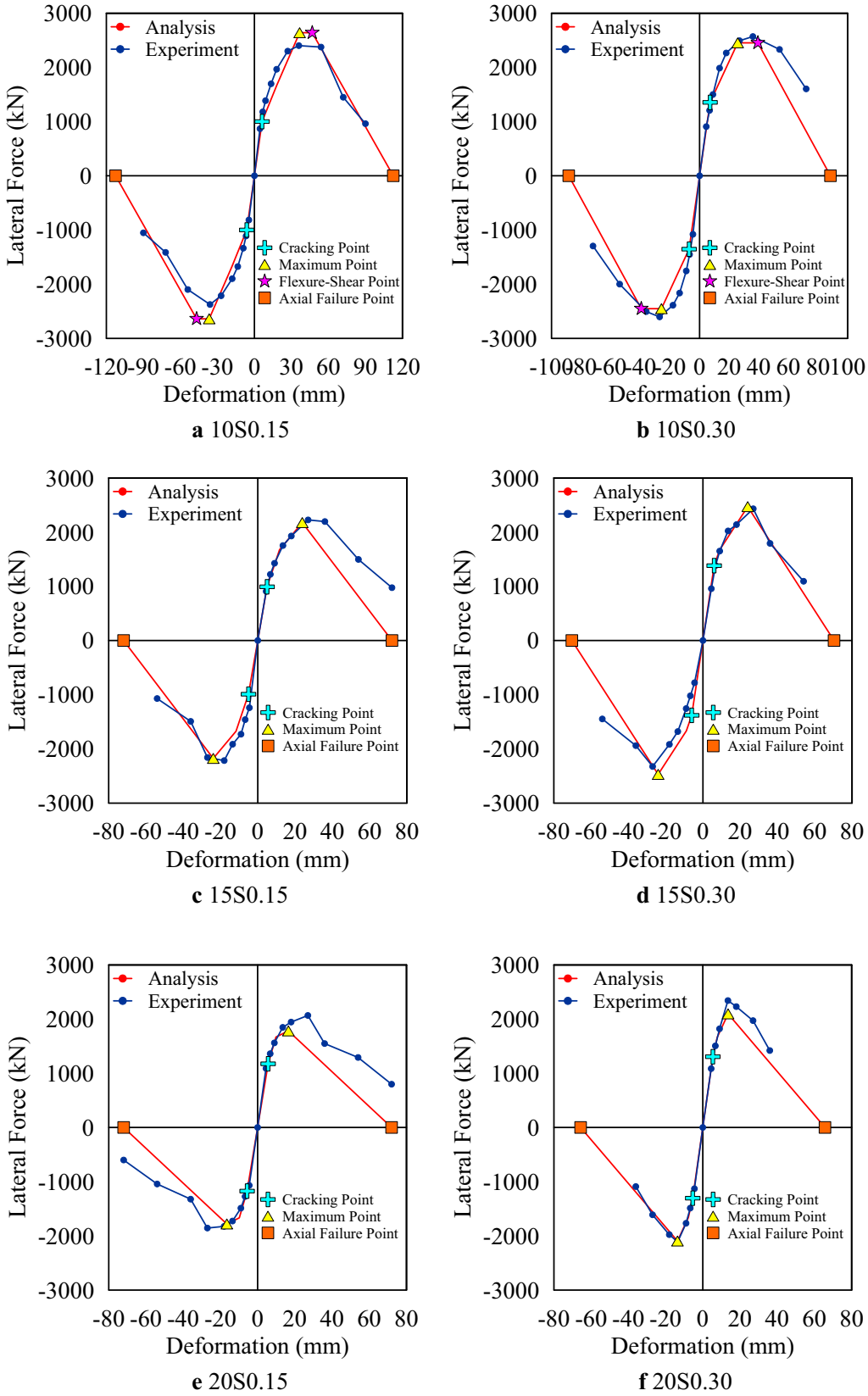

Fig. 18 Comparison of backbone curve between analysis and experimental results.

Table 9 Comparison of measured and predicted force at the cracking point.

Specimen	Measured force (kN)	Predicted force (kN)	Measured force/ predicted force
10S0.15	1180	1001	1.18
10S0.30	1500	1355	1.11
15S0.15	1221	992	1.23
15S0.30	957	1382	0.69
20S0.15	1090	1175	0.93
20S0.30	1086	1306	0.83

Table 10 Comparison of measured and predicted force at the maximum point.

Specimen	Measured force (kN)	Predicted force (kN)	Measured force/ predicted force
10S0.15	2403	2641	0.91
10S0.30	2571	2454	1.05
15S0.15	2226	2177	1.02
15S0.30	2432	2471	0.98
20S0.15	2068	1783	1.16
20S0.30	2343	2097	1.12

relevant experimental results. The unloading stiffness of an HSRC column member under cyclic loading, K_h, is assumed to be given by Eq. (18), based on the research by Chiu et al. (2015). In this work, the unloading stiffness function is regressed as shown in Eq. (19). Figure 19 compares the measured and predicted unloading stiffness.

$$\frac{K_h}{K_{cr}} = c_1 \left(\frac{\Delta}{\Delta_{cr}} \right)^{c_2} \tag{18}$$

where c_1 and c_2 are the parameters that are obtained from experimental results.

$$\frac{K_h}{K_{cr}} = 1.3 \left(\frac{\Delta}{\Delta_{cr}} \right)^{-0.65}. \tag{19}$$

4 Determination of Damage Level for HSRC Columns

A simple analytical model is introduced to capture the relationship between maximum residual crack and residual deformation. Maeda and Kang (2009) found that the deformation of a column can be assumed to comprise flexural and shear deformation, as given by Eq. (20). Figure 20 plots the geometric relationship between widths of residual flexural/shear cracks and residual flexural/shear deformation.

$$R_r = R_{rf} + R_{rs} \tag{20}$$

where R_{rf} is the deformation induced by residual flexural cracks and R_{rs} is the deformation induced by residual shear cracks.

The summation of residual flexural crack widths on both ends of a member, $\sum W_f$, can be used to estimate the deformation that is induced by residual flexural cracks. For convenience, n_f, which is a ratio of the maximum residual flexural crack width, $W_{f,max}$, to the total residual flexural crack widths, $\sum W_f$, is used to quantify the deformation of residual flexural cracks (Maeda and Kang

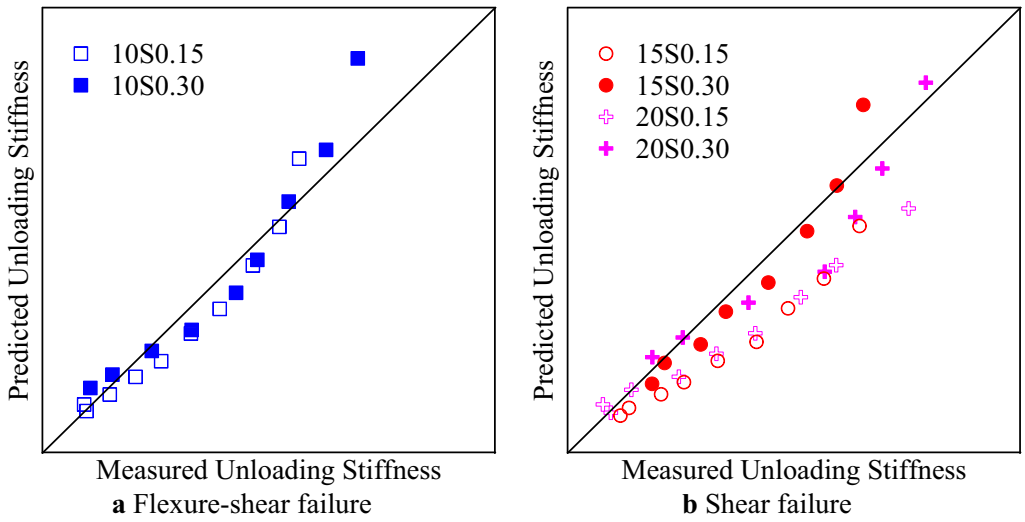

Fig. 19 Comparison of the measured and predicted unloading stiffness.

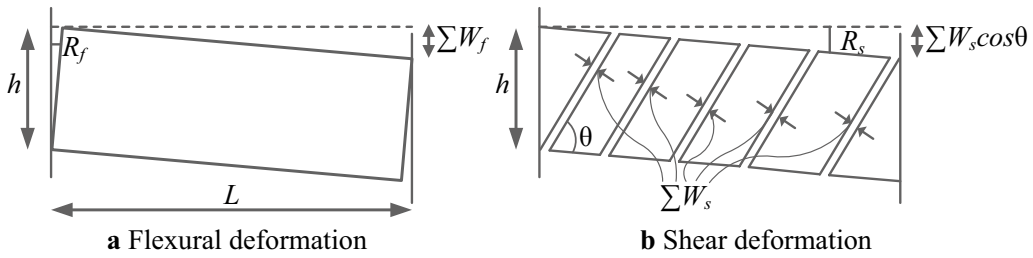

Fig. 20 Relationship between residual flexural/shear crack width and residual flexural/shear deformation.

2009). Experimental results indicate that n_f is approximately 2.0 for the HSRC column members with flexural–shear and shear failure modes. Additionally, Eq. (21) uses a ratio α_f, which is defined as the residual flexural deformation to the residual total deformation of a member, to quantify the residual total deformation of a member.

$$R_r = R_{rf} \times \frac{1}{\alpha_f} = \left(\frac{\sum W_f}{h - x_n}\right) \times \frac{1}{\alpha_f} = \left(\frac{n_f \times W_{f,\max}}{h - x_n}\right) \times \frac{1}{\alpha_f} \tag{21}$$

where x_n is the depth of neutral axis in section.

If the residual deformation of a member is dominated by shear cracking, then the residual shear deformation can be used to estimate the residual total deformation. The relationship between the residual shear crack width and residual shear deformation can be derived as for a flexural crack. The residual shear deformation that is caused by residual shear cracks can be estimated as n_s, which is a ratio of the maximum residual shear crack width, $W_{s,max}$, to the total residual shear crack widths, $\sum W_s$. Experimental results show that n_s value is nearly 3.0 for the HSRC column members with flexure–shear and shear failure modes. Applying the concept that was applied in Eq. (21), the residual total deformation of a member can be estimated using Eq. (22) and the residual shear deformation.

$$\begin{aligned} R_r &= R_{rs} \times \frac{1}{\alpha_s} = \left(\frac{2\sum W_s \cos\theta}{L}\right) \times \frac{1}{\alpha_s} \\ &= \left(\frac{2n_s \times W_{s,\max} \cos\theta}{L}\right) \times \frac{1}{\alpha_s} \end{aligned} \tag{22}$$

where θ is the angle of shear crack. Figure 21 plots n_f and n_s value which are obtained from experimental results.

Based on the relevant experimental results, since shear cracks develop more than flexural cracks, Eq. (22) is used to estimate the ratio of the residual shear deformation to the residual total deformation of a column member. Restated, the residual shear deformation can be calculated from the residual shear crack width, which was measured during the experiment, and Eq. (22). Experimental data are used herein to evaluate the ratio α_s in Eq. (22). Figure 22 shows the development of residual shear deformation and residual total deformation and

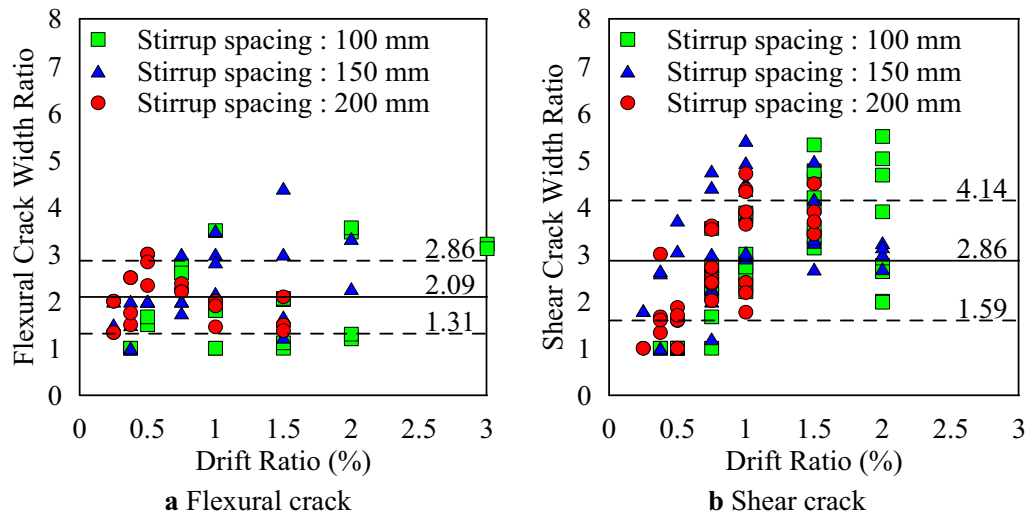

Fig. 21 Ratio of maximum residual crack width to total residual crack width.

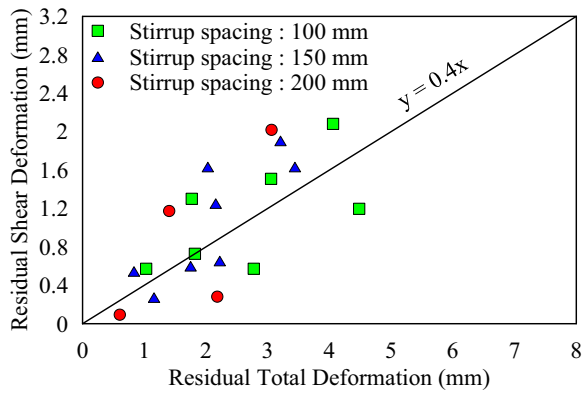

Fig. 22 Ratio of residual shear deformation to residual total deformation.

Table 11 Measured and predicted force at residual shear crack width of 0.15 mm.

Specimen	Measured force (kN)	Predicted force (kN)	Measured force/ predicted force
10S0.15	2005	1159	1.73
10S0.30	2409	1529	1.58
15S0.15	1608	1238	1.30
15S0.30	1551	1559	0.99
20S0.15	1569	1321	1.19
20S0.30	1948	1539	1.27

α_s value can be set to 0.4. Additionally, the residual total deformation that is calculated using Eq. (22) includes the deformations that are induced by the bond slipping of the longitudinal bars and the pullout displacement of the longitudinal bars from the foundation.

To identify the performance point that is related to a specified maximum residual flexural or shear crack width in the backbone curve of a column member, the unloading stiffness and residual deformation are used to, as shown in Fig. 22. The corresponding force at a specified crack width is calculated using Eq. (23). Meanwhile, Eq. (19) is used to determine the unloading stiffness. Tables 11, 12 and 13 present the calculated forces at the corresponding crack width of 0.15 mm, 0.30 mm, and 1.00 mm respectively.

$$V = \frac{K_2(\Delta_r - \Delta_{cr}) + V_{cr}}{\left(1 - \frac{K_2}{K_h}\right)} \tag{23}$$

where V is the lateral force related to a specified crack width; K_2 is the slope between the cracking point and the maximum point; Δ_r is the residual deformation related to a specified crack width; Δ_{cr} is the deformation at cracking point; V_{cr} is the cracking strength; K_h is the unloading stiffness (Fig. 23).

Table 12 Measured and predicted force at residual shear crack width of 0.30 mm.

Specimen	Measured force (kN)	Predicted force (kN)	Measured force/ predicted force
10S0.15	2222	1822	1.22
10S0.30	2551	2081	1.23
15S0.15	1929	2087	0.92
15S0.30	2023	2179	0.93
20S0.15	1761	1679	1.05
20S0.30	2160	1859	1.16

Table 13 Measured and predicted force at residual shear crack width of 1.00 mm.

Specimen	Measured force (kN)	Predicted force (kN)	Measured force/ predicted force
10S0.15	2282	2485	0.92
10S0.30	2563	2268	1.13
15S0.15	2200	1643	1.34
15S0.30	2432	1922	1.27
20S0.15	1835	1429	1.28
20S0.30	2231	1690	1.32

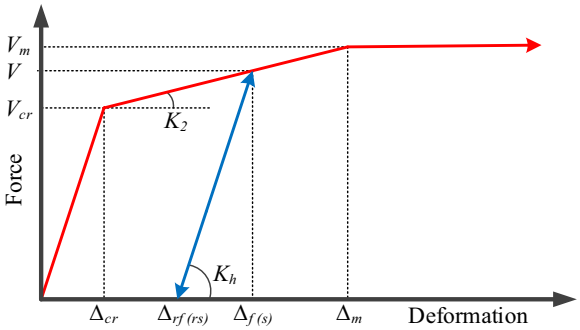

Fig. 23 Relationship between residual deformation and peak deformation.

The relationship between lateral force and residual crack width is obtained. This relationship can help engineers to identify the damage level in the post-earthquake performance assessment. Figure 24 plots the relationship between lateral force and residual crack width.

To ensure reparability under short-term loading that is caused by a medium-magnitude earthquake, AIJ (2010) recommended a maximum residual shear crack width of 0.30 mm. According to experimental results, the specimens with flexure–shear failure, which are 10S0.30 and 10S0.15, reach their maximum strength at a residual

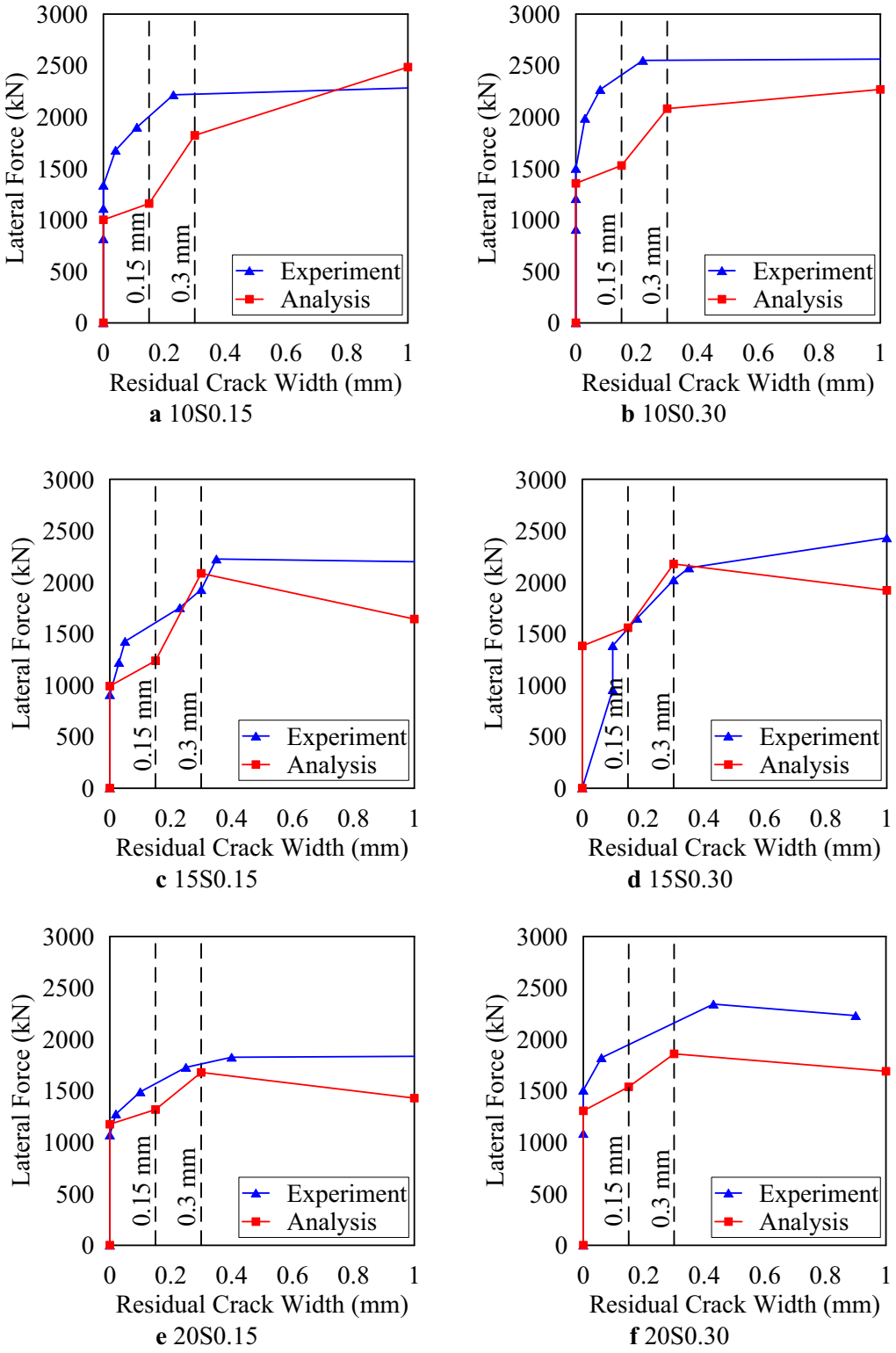

Fig. 24 Relationship between lateral force and residual crack width.

shear crack width of less than 0.30 mm. Specimens that undergo shear failure have not reached their maximum strength when the residual shear crack width is 0.30 mm. Therefore, increasing the number of transverse reinforcements can reduce the maximum shear crack width while maintaining maximum strength. Meanwhile, the calculated results yield a more conservative value of force than the experimental results, except for the specimen 15S0.30 which had a twisting moment during loading. Some relatively large differences are observed between the flexure–shear specimens 10S.30 and 10S0.15, especially in early stages of loading.

Based on the experimental results in Table 6, a maximum residual crack width of 0.15 mm is specified as the value that separates damage levels I (DLI) and II (DLII), and it is denoted as the operational limit point, cR_1. The deformation, defined as repair limit I, cR_2 in the backbone curve, that corresponds to the point that separates damage levels II and III (DLIII), is calculated using a maximum residual crack width of 0.30 mm. Repair limit I for specimens with a relatively high axial load are determined by shear cracking (R_{s2}) because the axial load helps to close the flexural cracks. In addition to the maximum residual crack width of 1.0 mm, the maximum strength of a column member is used to determine the dividing point between damage levels III and IV (DLIV)—repair limit II, cR_3. Obviously, the maximum strength of a column member governs the dividing point between DLIII and DLIV for each specimen. The maximum strength of a column member multiplied by 0.8 or the axial failure point is used to define the point that separates damage levels IV and V (DLV)—the collapse limit point, cR_4. Table 14 presents the performance points for each specimen and the points that separate the damage levels.

Table 15 shows the average values of the separating points that are obtained from the analysis and experimental results. The results of the analysis of the specimens with flexure–shear and shear failure modes differ slightly from the experimental results. For cR_2 and cR_3, although the drift ratios that are obtained by analysis exceed the measured drift ratios, the difference between

Table 14 Calculated dividing point for each damage level.

Deformation of a member	Specimen					
	10S0.15 (%)	10S0.30 (%)	15S0.15 (%)	15S0.30 (%)	20S0.15 (%)	20S0.30 (%)
Dividing point between DLI and DLII						
cR_1	0.50	0.56	0.47	0.50	0.46	0.43
Dividing point between DLII and DLIII						
R_{f2}	1.14	1.12	1.23	1.09	0.82	1.01
R_{s2}	1.19	1.08	1.25	1.07	0.82	0.62
cR_2	1.14	1.08	1.23	1.07	0.82	0.62
Dividing point between DLIII and DLIV						
R_{f3}	2.77	2.46	1.97	1.95	1.53	1.65
R_{s3}	2.82	2.39	1.98	1.91	1.53	1.32
V_{max}	2.04	1.43	1.32	1.33	0.92	0.76
cR_3	2.04	1.43	1.32	1.33	0.92	0.76
Dividing point between DLIV and DLV						
0.8 V_{max}	3.33	2.73	1.86	1.85	1.54	1.33
R_{a4}	6.25	4.91	4.00	3.91	4.00	3.65
cR_4	3.33	2.73	1.86	1.85	1.54	1.33

Table 15 Measured and predicted drift ratio for each dividing point.

Dividing point	Flexure–shear failure		Shear failure	
	Measured (%)	Predicted (%)	Measured (%)	Predicted (%)
cR_1	0.75	0.53	0.47	0.47
cR_2	1.00	1.11	0.69	0.93
cR_3	1.50	1.74	1.38	1.08
cR_4	3.43	3.03	1.99	1.64

Table 16 Suggested drift ratio for each damage level.

Damage level	Suggested value	
	Flexure–shear failure	Shear failure
I	< 0.50%	< 0.30%
II	0.50–1.00%	0.30%–0.60%
III	1.00%–Δ_{Vmax}	0.60%–Δ_{Vmax}
IV	Δ_{Vmax}–$\Delta_{0.8Vmax}$	Δ_{Vmax}–$\Delta_{0.8Vmax}$
V	> $\Delta_{0.8Vmax}$	> $\Delta_{0.8Vmax}$

Δ_{Vmax} is the drift ratio at maximum strength of member and $\Delta_{0.8Vmax}$ is the drift ratio at 80% of maximum strength of member

them is less than 0.3%. Therefore, the proposed method can still be used to quantify the damage for the HSRC column members with flexure–shear and shear failure modes. For the convenience in engineering, Table 16 suggests the drift ratio limits of each damage level for HSRC column members with flexure–shear and shear failure modes.

This work also proposes a damage evaluation method for HSRC column. Based on the suggested value in Table 6, this method integrates force–deformation relationship, force-residual crack width relationship, and evaluation of damage level based on crack width and deformation. Based on Fig. 1, the top-right quadrant (I) presents the force–deformation relationship. It also illustrates the damage level position on the force–deformation curve. The top-left quadrant (II) shows the relationship between the lateral force and the residual shear crack width. This curve can identify the damage level of a structure in the post-earthquake performance assessment. The relationship between maximum residual crack width and the damage level is presented in the bottom-left quadrant (III). The curve is defined by the proposed value of residual crack width in Table 6. The bottom-right quadrant (IV) shows the relationship between deformation of a member and its corresponding damage level. Using this curve, engineers can set an allowable damage level to determine the corresponding deformation. Therefore, the proposed damage assessment method can allow engineers to engage performance-based design for HSRC column.

Figures 25 and 26 plot the damage evaluation method for flexure–shear failure specimens whereas Figs. 27, 28, 29 and 30 plot the damage evaluation method for shear failure specimens. Overall, specimens with relatively high axial load start to develop cracks when the lateral force is 60% of their maximum strength on average, while specimens with relatively small axial load start to develop cracks when the lateral force is 40% of their maximum strength on average.

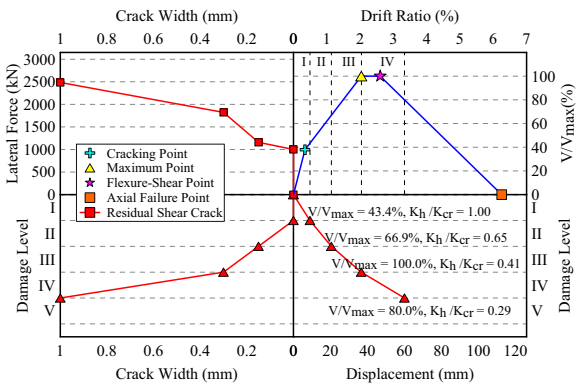

Fig. 25 Damage assessment for specimen 10S0.15.

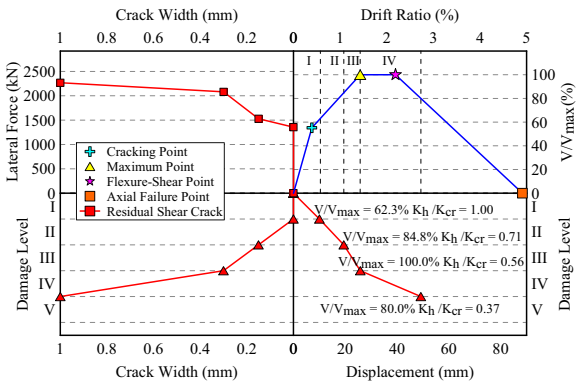

Fig. 26 Damage assessment for specimen 10S0.30.

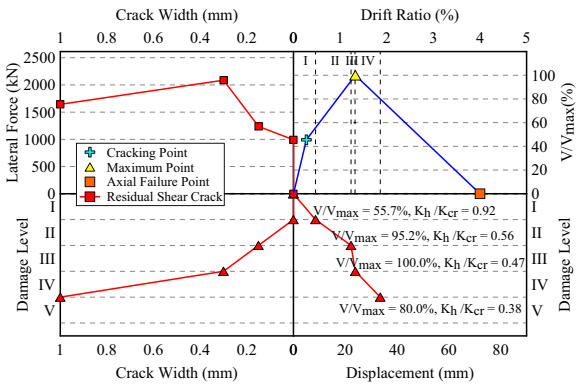

Fig. 27 Damage assessment for specimen 15S0.15.

It also can be estimated that specimens with flexure–shear failure, 10S0.15 and 10S0.30, along with specimen 15S0.15 and 15S0.30, develop residual shear crack width of 0.30 mm at a deformation of more than 1%. On the other hand, specimen with a relatively low amount of transverse reinforcements, 20S0.15 and

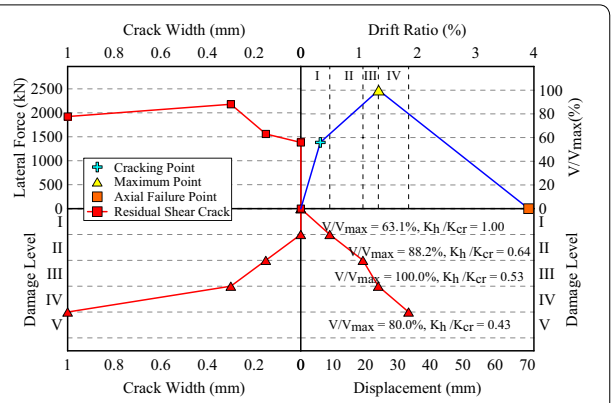

Fig. 28 Damage assessment for specimen 15S0.30.

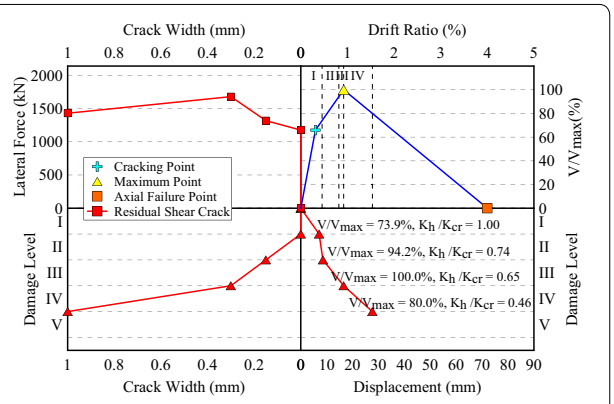

Fig. 29 Damage assessment for specimen 20S0.15.

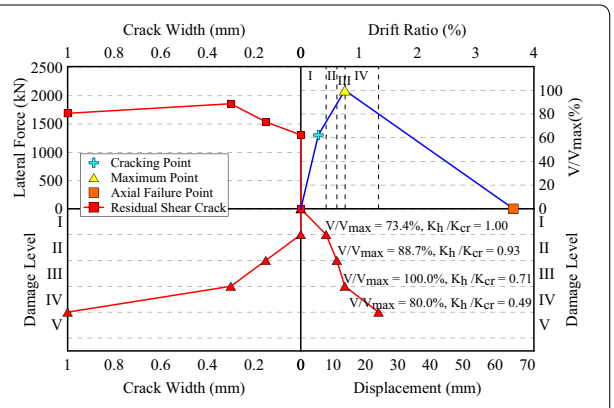

Fig. 30 Damage assessment for specimen 20S0.30.

20S0.30, develop the same residual shear crack width at a deformation of less than 1%. Notably, even specimen 10S0.15, 10S0.30, 15S0.15, and 15S0.30 have approximately similar deformation at the residual shear crack width of 0.30 mm, specimen 15S0.15 and 15S0.30, which categorized as shear failure specimens, generate a rapid development of lateral force, 90% of maximum strength on average, compared to 70% of maximum on average on flexure–shear failure members. Furthermore, the collapse limit points are marked on 80% of maximum strength for all specimens. The amount of transverse reinforcements is a controlling factor for this point. The collapse limit points of flexure–shear failure specimens are estimated at 3% deformation on average, while the collapse limit point of shear failure specimens is estimated at 1.5% deformation.

5 Conclusion

In this paper, the basic concept and method for evaluating the damage level of HSRC column are presented. Six full-size columns are tested under lateral and axial loading. Based on the damage pattern, the failure mechanism can be categorized into flexure–shear failure and shear failure. Experiment results show that the flexure–shear failure members reach their maximum strength before their main bars yield, while shear failure members reach their maximum strength after their main bars yield. It is also clear that the axial load ratio is crucial for estimating the column drift capacity. The drift capacity decreases by increasing the axial load ratio. Meanwhile, shear cracks are observed to develop more severe than flexural cracks. Based on the average value of the maximum residual crack width, the limiting value of maximum residual crack width for each damage level is used as shown in Table 6.

An analytical backbone curve model for predicting the force–deformation behavior of HSRC column is also described. The proposed backbone curve for flexure–shear failure comprises four points; cracking, maximum strength, flexure–shear failure, and axial load failure. On the other hand, the proposed backbone curve for shear failure consists of three points; cracking, maximum strength, and axial load failure. Good agreement between the proposed model and experiment results is observed as the proposed model produces more conservative results. Additionally, to understand the behavior of HSRC column under cyclic loading, the unloading stiffness of each specimen is observed and a simplified formula is also suggested based on experiment results.

Moreover, a damage assessment method for HSRC column is also introduced. This work uses dividing points based on a specified residual crack width of 0.15 mm, 0.30 mm, and 1.00 mm to determine the damage level of structures. The average values of the dividing points are listed in Table 15, for both measured and predicted results. Then, a new drift ratio limit of each damage level is also proposed in Table 16. Overall, this work integrates force–deformation relationship, deformation–damage level relationship, force–crack width relationship, and

crack width–damage level to evaluate the performance of HSRC columns. As for future research, much work and more experiments are, however, necessary to improve the accuracy of the proposed method.

Acknowledgements
Not applicable.

Authors' contributions
C-KC is responsible to interpret the experiment data, arranged the manuscript outline, and is the primary contributor in writing the manuscript. AIT involves during the experiment and performed the analysis. All authors agree both to be accountable for their own contributions and to ensure that questions related to the accuracy or integrity of any part of the work, even ones in which the author is not personally involved, are appropriately investigated, resolved, and the resolution documented in the literature. Both authors read and approved the final manuscript.

Authors' information
Mr. Chien-Kuo Chiu is currently working as Professor in the Department of Civil and Construction Engineering at College of Engineering affiliated to National Taiwan University of Science and Technology, Taipei, Taiwan. He got his Ph.D. degree from The University of Tokyo, Tokyo, Japan. He has more than 10 years of experience in teaching in the field of RC structures. His research interests include the mechanic behavior simulation of high-strength RC beams and columns. He has published more than 50 papers in international conference and journals.

Mr. Alexander Ivan Tandri is currently a 4th year doctoral student in the Department of Civil and Construction Engineering at National Taiwan University of Science and Technology, Taipei, Taiwan. His research work is focused on the mechanical performance assessment of high-strength RC column members.

Funding
The research is funded by Ministry of Science and Technology, Taipei, Taiwan (MOST) and the Project number is MOST 107-2625-M-011-001.

Availability of data and materials
All data generated or analyzed during this study are included in this published article. Additional data for further discussions are available from the corresponding author on request.

Competing interests
The authors declare that they have no competing interests.

Received: 21 November 2019 Accepted: 23 March 2020
Published online: 18 June 2020

References

ACI 318-19. (2019). *Building code requirements for structural concrete and commentary*. Farmington Hills: American Concrete Institute.
ACI 363R-10. (2010). *Report on high-strength concrete*. Farmington Hills: American Concrete Institute.
AIJ. (2010). *Standard for structural calculation of reinforced concrete structures*. Tokyo: Architectural Institute of Japan.
Chang, F.C. (2010). *Study on the confining effect of reinforced concrete columns using high strength materials*. Thesis, National Taiwan University.
Chiu, C. K., Chi, K. N., & Lin, F. C. (2014). Experimental investigation on the shear crack development of shear-critical high-strength reinforced concrete beams. *Journal of Advanced Concrete Technology, 12*(7), 223–238.
Chiu, C. K., Ferry, F. M., & Darwin, S. (2015). Crack-based damage assessment method for HSRC shear-critical beams and columns. *Advances in Structural Engineering, 18*(1), 119–135.
Chiu, C. K., Sugianto, S., Liao, W. I., & Ho, C. E. (2019). Crack-based damage quantification for shear-critical HSRC column members using piezoceramic transducers. *Engineering Structures, 201*, 109777.
Elwood, K. J., & Moehle, J. P. (2005). Axial capacity model for shear-damaged columns. *ACI Struct J, 102*(4), 578–587.
FIP/CEB. (1990). *Strength concrete, State of the Art Report*. Lausanne: Coomitte Euro-International du Beton.
JBDPA. (2001). *Guideline for post-earthquake damage evaluation and rehabilitation*. Tokyo: Japan Building Disaster Prevention Association.
JBDPA. (2015). *Standard for seismic evaluation of existing reinforced concrete buildings, guidelines for seismic retrofit of existing reinforced concrete buildings, and technical manual for seismic evaluation and seismic retrofit of existing reinforced concrete buildings*. Tokyo: Japan Building Disaster Prevention Association.
Maeda, M., & Kang, D. E. (2009). Post-earthquake damage evaluation for reinforced concrete buildings. *Journal of Advanced Concrete Technology, 7*(3), 327–335.
Maekawa, K., & An, X. (2000). Shear failure and ductility of RC columns after yielding of main reinforcement. *Engineering Fracture Mechanics, 65*, 335–368.
NCREE. (2017). *Design guideline for high-strength reinforced concrete structures*. Taipei: National Center for Research on Earthquake Engineering of Taiwan.
Patwardhan, C. (2005). *Shear strength and deformation modelling of reinforced concrete column*. Thesis, Ohio State University.
Santoro, M. G., & Kunnath, S. K. (2013). Damage-based RC beam element for nonlinear structural analysis. *Engineering Structures, 49*, 733–742.
Setzler, E.J. (2005). *Modeling the behavior of lightly reinforced concrete columns subjected to lateral loads*. Thesis, Ohio State University.
Sezen, H. (2002). *Seismic behavior and modelling of reinforced concrete building columns*. Dissertation, University of California.
Yoshimura, M., & Takaine, Y. (2005). Formulation of post-peak behavior of reinforced concrete columns including collapse drift. *Japan Structural Construction Engineering, 587*, 163–171.

Publisher's Note